Seasonal surface chlorophyll *a* variability in the Seychelles–Chagos Thermocline Ridge

Jenson V. George[1,*], M. Nuncio[2], N. Anilkumar[2], Racheal Chacko[2] and D. Rajashekhar[1]

[1]National Institute of Ocean Technology, Chennai 600 100, India
[2]National Centre for Antarctic and Ocean Research, Goa 403 804, India

Seychelles–Chagos Thermocline Ridge (SCTR, 5°–10°S, 50°–75°E) in the southwestern tropical Indian Ocean is a unique area that experiences year-round upwelling. This is a response to the upward Ekman pumping prevalent in the region. Satellite data, model data and objectively analysed Argo temperature/salinity data have been used to study the seasonal surface chlorophyll *a* (chl *a*) variability in SCTR. Variability of surface chl *a* concentration in SCTR showed a weak semiannual signature. The western part of SCTR (WSCTR, 50°–62°E) is characterized by higher chl *a* concentration than the eastern part (ESCTR, 63°–75°E). Average chl *a* concentration in WSCTR/ESCTR showed a primary peak in July–August (~0.26/~0.16 mg/m^3) and a secondary peak in January (~0.14/~0.12 mg/m^3). Minimum chl *a* concentration (~0.12/~0.1 mg/m^3) was observed during March–April and December–January. The high amplitude of chl *a* variability observed during July–August is associated with weak stratification and deep mixed layer depth (MLD). Deep MLD reaching to nutrient-rich thermocline entrains nutrients to the surface and thereby increases the surface chl *a* concentration. However, the low surface chl *a* concentration is a result of shallow MLD in the region. The deep MLD (30–40 m) observed during June–October is dominated by wind mixing and supported by buoyancy mixing. Shallow MLD (<30 m) observed during rest of the year is due to weak wind mixing and high surface buoyancy. The high surface buoyancy is a manifestation of ocean surface warming and presence of low saline surface waters in the SCTR region.

Keywords: Buoyancy flux, chlorophyll *a*, climatology, wind mixing.

THE Seychelles–Chagos Thermocline Ridge (SCTR, 5°–10°S, 50°–75°E) is an area that experiences year-round upwelling in the southwestern tropical Indian Ocean[1,2]. The climatological annual mean thermocline depth here is less than 70 m. This shallow thermocline is maintained by the upward Ekman pumping due to wind curl between equatorial westerlies and southeasterly trade winds[3]. Other than wind curl, beta effect and Rossby waves also have an influence on the thermocline depth in SCTR[4,5]. The region is part of the shallow meridional overturning circulation, which connects subtropical and tropical Indian Ocean[6]. The shallow thermocline and year-round upwelling make the SCTR an important region for biological productivity[7]. Shallow thermocline favours chlorophyll *a* (chl *a*) blooms, as there are more chances of entrainment or vertical advection of nutrient-rich thermocline waters to the surface[8]. Generally, near-surface layers of stratified oceans are nutrient-limited because of its uptake by phytoplankton, export of organic matter and low diffusive nutrient supply from greater depths[9].

An earlier study using the SeaWiFS chl data observed surface chl *a* blooms in the southern tropical Indian Ocean and suggested that they were associated with the thermocline ridge and regulated by mixed layer depth (MLD) variability[10]. A recent study suggested that entrainment of chl *a* from the deep chlorophyll maxima (DCM) to the surface can increase the surface chl *a* concentration in the region[11]. The model employed by Resplandy *et al.*[8] suggests that in SCTR, nutrients entrained to surface due to wind-induced mixing can also result in elevated chl *a* concentration. Waliser *et al.*[12] discussed the influence of Madden–Julian Oscillation (MJO)-induced wind bursts on chl *a* blooms. They also linked the blooms in SCTR to the deepening of MLD. Kawamiya and Oschlies[5] pointed out that the annual Rossby waves from the east have considerable effect on chl *a* distribution in SCTR. Jayakumar and Gnanaseelan[13] using an Ocean General Circulation Model (OGCM) suggested that intraseasonal dynamic response and interannual forcing are responsible for the blooms in the southwestern tropical Indian Ocean. They showed that both Rossby waves and local upwelling lift phytoplankton from DCM to the surface creating a bloom. Daria and Tong[14] showed that in SCTR salinity varied on a seasonal and interannual scale, and suggested that meridional Ekman transport plays a role in this. However, studies detailing the role of salinity variability on MLD, stratification and its influence on surface chl *a* in the SCTR region are limited. Furthermore, spatial variability of surface chl *a* concentration within the SCTR has not been attempted so far. The main objective of this study is to assess the seasonal variation of chl *a* and its

*For correspondence. (e-mail: jensonvgeorge@gmail.com)

influencing factors in SCTR, using satellite and ARGO data.

Data and methods

The Argo-based, objectively analysed monthly mean temperature and salinity profiles from Japan Agency for Marine-Earth Science and Technology (JAMSTEC, January 2000 to January 2011) have been used to calculate climatology in the tropical Indian Ocean. The large deviations (larger than three times the standard deviation at each depth level) from the world ocean dataset 2001 (ref. 15) observed in the individual Argo profiles were treated as bad profiles and not used to calculate the monthly objectively analysed temperature and salinity profiles. Further details of data processing and interpolation are given in Shigeki *et al.*[16]. Monthly sea-viewing wide field-of-view sensor (SeaWiFS) chl *a* (December 1997 to December 2010), quick scatterometer (QuikSCAT) winds (August 1999 to October 2009) and Aqua Moderate Resolution Imaging Spectroradiometer (MODIS) photosynthetically active radiation (PAR, August 2002 to August 2012) from Environmental Research Division's Data Access Program (ERDDAP)[17], were used to calculate monthly climatology of the respective variables. The monthly rain rate (January 1998 to January 2012) from Tropical Microwave Imager (TMI, http://www.remss.com) and sea-level anomaly (SLA, October 1992 to April 2012) from AVISO live access server (http://atoll-motu.aviso.oceanobs.com) were also used to calculate monthly climatology in the present study. Surface ocean current monthly climatology was calculated using Ocean Surface Current Analysis–Real-time (OSCAR, October 1992 to October 2012, http://www.oscar.noaa.gov) data[18]. The monthly climatology of net heat flux was derived from gridded OAFlux[19] (Objectively Analyzed air–sea Fluxes, http://oaflux.whoi.edu) data spanning from January 1998 to December 2008. To sustain the observations made by the satellites, CTD (SBE 19plus, USA) data from the upper 200 m water column, collected at 8°S, 65°E during November 2008 and June 2009 were used. Sea-water samples were also collected from 11 depths (0, 10, 20, 30, 50, 75, 100, 120, 150, 180 and 200 m) at this location using the CTD rosette system (Idronaut, Italy) fitted with 24 Niskin bottles, each of 1.75 l capacity. The chl *a* concentration was estimated following the method of Strickland and Parsons[20]. Water samples for nitrate measurements were collected in clean polypropylene bottles and analysed using a Skalar auto analyser.

The Ekman pumping velocity was calculated following Weller *et al.*[21]

$$w_{\mathrm{EP}} = \frac{1}{f\rho_0}\left(\nabla \times \bar{\tau}_0 + \frac{\beta}{f}\tau_0^x\right), \tag{1}$$

where $\bar{\tau}_0 = (\tau_0^x, \tau_0^y)$ is the surface wind stress, ρ_0 the reference sea-water density (1025 kg m^{-3}), f the Coriolis force and β is a measure of its variation with latitude. Brunt–Vaisala frequency was calculated following Pond and Pickard[22]. MLD was calculated based on 0.2 kg m^{-3} density difference criterion from the first depth level (~10 m) ARGO density data. Net buoyancy flux B_0 was calculated as the sum of thermal buoyancy flux B_q and haline buoyancy flux B_s following Gill[23]

$$B_0 = B_q + B_s,$$

$$B_0 = \left(\frac{g\alpha Q_0}{\rho C_p}\right) + g\beta(E-P)S_0, \tag{2}$$

where g is the acceleration due to gravity, α the thermal expansion coefficient, β the haline contraction coefficient, C_p the specific heat capacity of water, Q_0 the net heat flux, E the evaporation rate, S_0 the surface salinity and P is the precipitation rate. Monin–Obhukov length L was computed following Gill[23]

$$L = -\left(\frac{U_*^3}{kB_0}\right), \tag{3}$$

where Von Karman constant $k = 0.41$. Friction velocity U_* was calculated from surface wind stress using

$$U_* = \left(\frac{\tau_0}{\rho}\right)^{1/2}. \tag{4}$$

Results and discussion

Figure 1 *a* shows the average of annual climatology of objectively analysed gridded temperature profiles in the SCTR region (50°–75°E and 5°–10°S). Figure 1 *b* shows the sea truth CTD temperature and salinity profiles collected from 8°S, 65°E during November 2008 when thermocline was shallow (25 m) and June 2009 when thermocline was deep (50 m). From Figure 1 *a* and *b*, it can be seen that in this upwelling region, the centre of thermocline is better represented by 23°C isotherm depth rather than the popularly used 20°C isotherm depth. Hence in the present study 23°C isotherm depth is treated as the thermocline depth. Using this criterion the annual mean thermocline depth over the SCTR region is ~60 m. Figure 2 shows the climatological thermocline depth <70 m overlaid on the climatological SeaWiFS chl *a* concentration. It can be seen that major part of this shallow thermocline region is restricted to the SCTR region. The shallow thermocline indicates active year-round upwelling and presence of nutrient-rich thermocline waters within the euphotic zone in the region[7]. Even though this

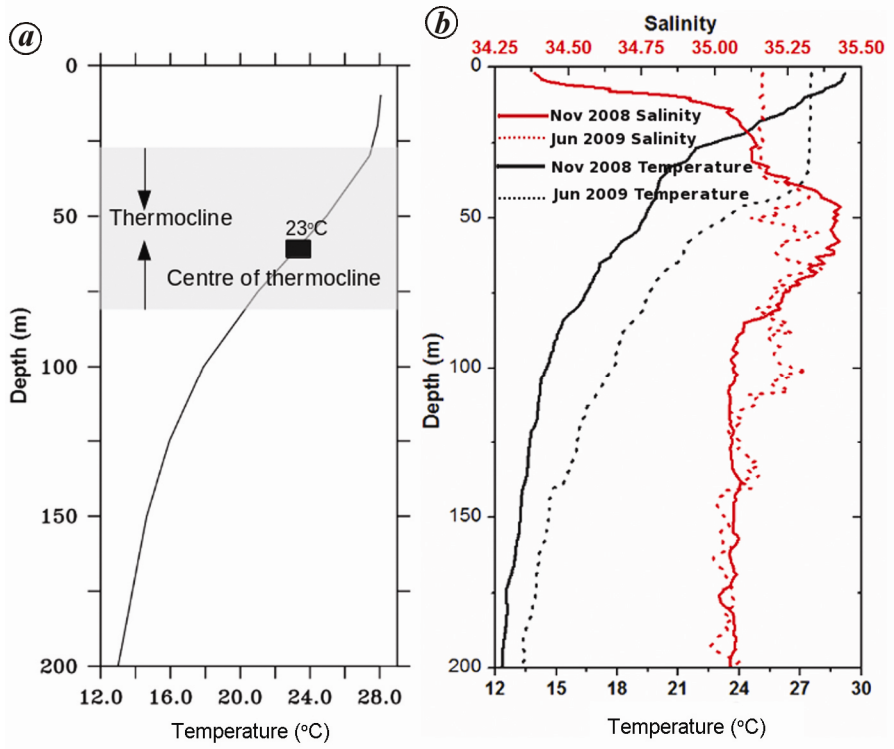

Figure 1. ***a***, Annual mean climatology of temperature profiles averaged over 50°–75°E and 5°–10°S in the Seychelles–Chagos Thermocline Ridge region. ***b***, Temperature (black line) and salinity (red line) profiles were collected using CTD at 8°S, 65°E during November 2008 (continuous line) and June 2009 (dashed line). The filled boxes represent the 23°C isotherm depth.

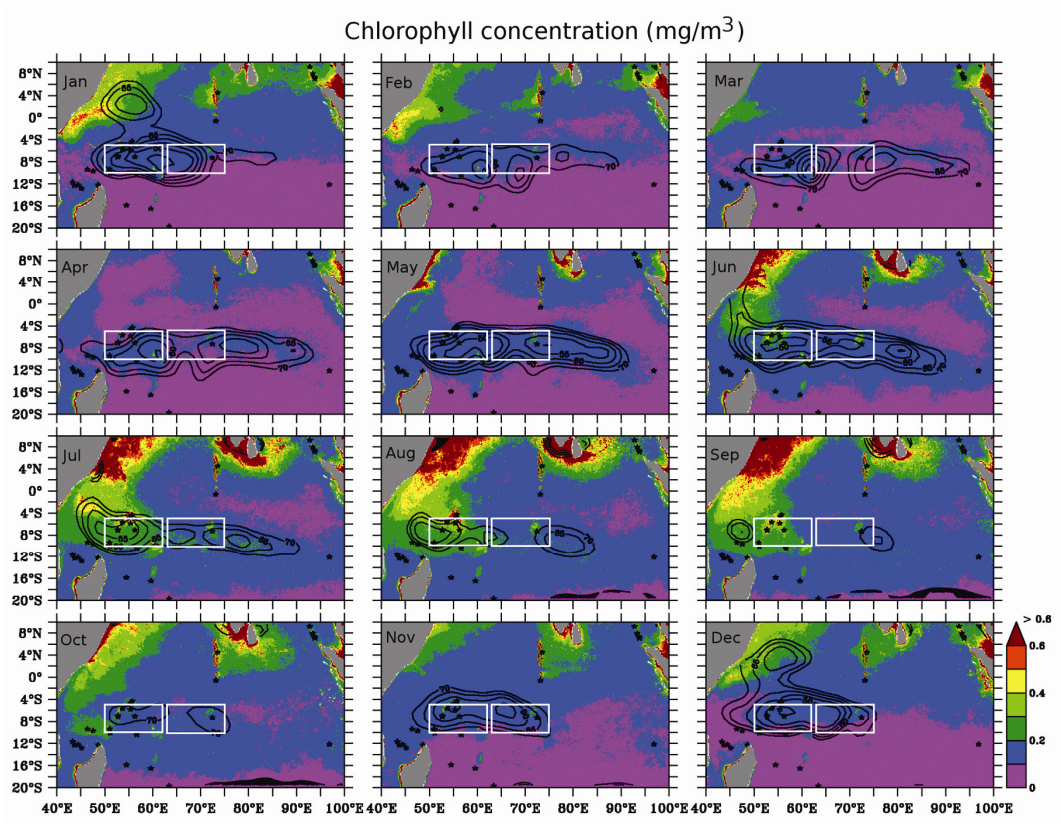

Figure 2. Monthly climatological SeaWiFS surface chl *a* distribution (mg/m^3) in the tropical Indian Ocean overlaid by the monthly climatological thermocline depth shallower than 70 m. The thermocline depth contour interval is 5 m. The white western box in the panel represents WSCTR and the white eastern box represents ESCTR. Stars represent the islands.

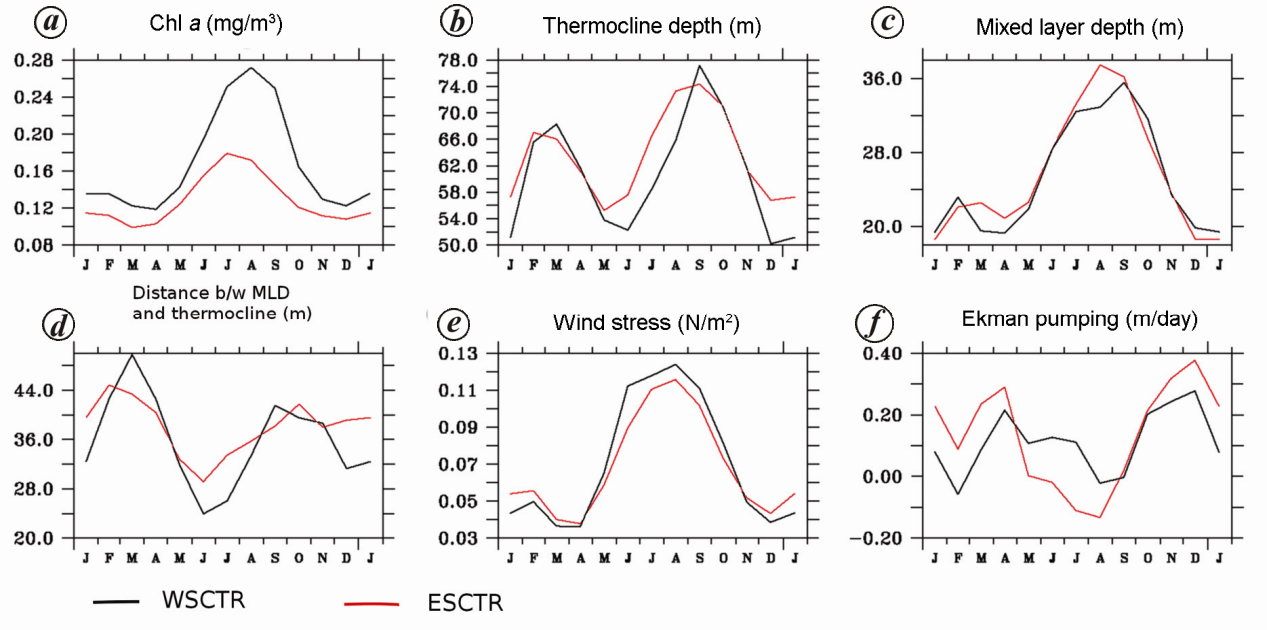

Figure 3. Annual variation of various parameters averaged over WSCTR (black line, 50°–62°E, 5°–10°S) and ESCTR (red line, 63°–75°E, 5°–10°S): ***a***, SeaWiFS surface chl *a* (mg/m^3); ***b***, thermocline depth (m); ***c***, mixed layer depth (MLD) (m); ***d***, distance between MLD and thermocline (m); ***e***, wind stress (N/m^2); ***f***, Ekman pumping (m/day).

region is characterized by year-round shallow thermocline, elevated surface chl *a* concentrations (>0.2 mg/m^3) are only noted from June to October (Figure 2). The western part of the SCTR (WSCTR, 50°–62°E) has higher chl *a* concentration than the eastern part (ESCTR, 63°–75°E). To understand the response of seasonal surface chl *a* to the various physical parameters, we constructed climatology of different physical properties and averaged it over WSCTR and ESCTR.

Figure 3 *a* shows the seasonal variability of averaged SeaWiFS surface chl *a* concentration in WSCTR and ESCTR. The remarkable feature is a weak semiannual signal in WSCTR/ESCTR with a primary maximum in July–August (~0.26/~0.16 mg/m^3) and secondary maximum in January (~0.14/~0.12 mg/m^3); again two minima (~0.12/~0.1 mg/m^3) are noted in March–April and December–January. The amplitude of seasonal variability of surface chl *a* in WSCTR is more than that in ESCTR. It is clear from the seasonal variation of thermocline depth averaged over WSCTR and ESCTR (Figure 3 *b*), that the strong semiannual variation in thermocline depth is not captured in the surface chl *a*. According to Resplandy *et al.*[8], shallow thermocline is a necessary but not sole condition for elevated surface chl *a* in SCTR; a deep MLD is also required to bring subsurface nutrients to the surface. The shallow thermocline (~50–54 m) in WSCTR and ESCTR during January did not result in a chl *a* peak. Figure 3 *c* shows the monthly climatological MLD derived from the objectively analysed ARGO data in the tropical Indian Ocean averaged over WSCTR and ESCTR. It can be seen that the MLD is deep (30–40 m) from June to October and shallow (<30 m) from November to May, coinciding with the high and low chl *a* periods respectively. Previous studies showed that surface chl *a* concentration in this region is regulated by MLD[8,10,24]. The seasonal variation of chl *a* follows a pattern similar to that of MLD. The distance between the base of mixed layer and centre of thermocline (Figure 3 *d*) depicts lowest values during June–August in WSCTR. A mixed layer close to the centre of thermocline can enhance the entrainment of nutrient-rich thermocline waters to the surface layers, which eventually can increase the surface chl *a* concentration. This may be one of the reasons for elevated surface chl *a* in WSCTR than ESCTR during June–August.

Seasonal variation of the magnitude of wind stress (Figure 3 *e*) has a similar pattern as that of MLD with slightly higher magnitude in WSCTR than in ESCTR during June–October and lower magnitude during rest of the year. Seasonal variation of Ekman pumping averaged over WSCTR (Figure 3 *f*) shows that Ekman pumping is upward (positive, indicating wind-induced upwelling) year round, except during February, August and September. However, in ESCTR Ekman pumping is downward (negative, indicating wind-induced downwelling) from May to September, while it is upward during rest of the year. One can notice that the seasonal progression of Ekman pumping has a pattern similar to that of thermocline depth both in WSCTR and ESCTR. However, there is some phase difference between thermocline depth and Ekman pumping variability (Figure 3 *b* and *f*). For example, during May–July when Ekman pumping is negative in ESCTR

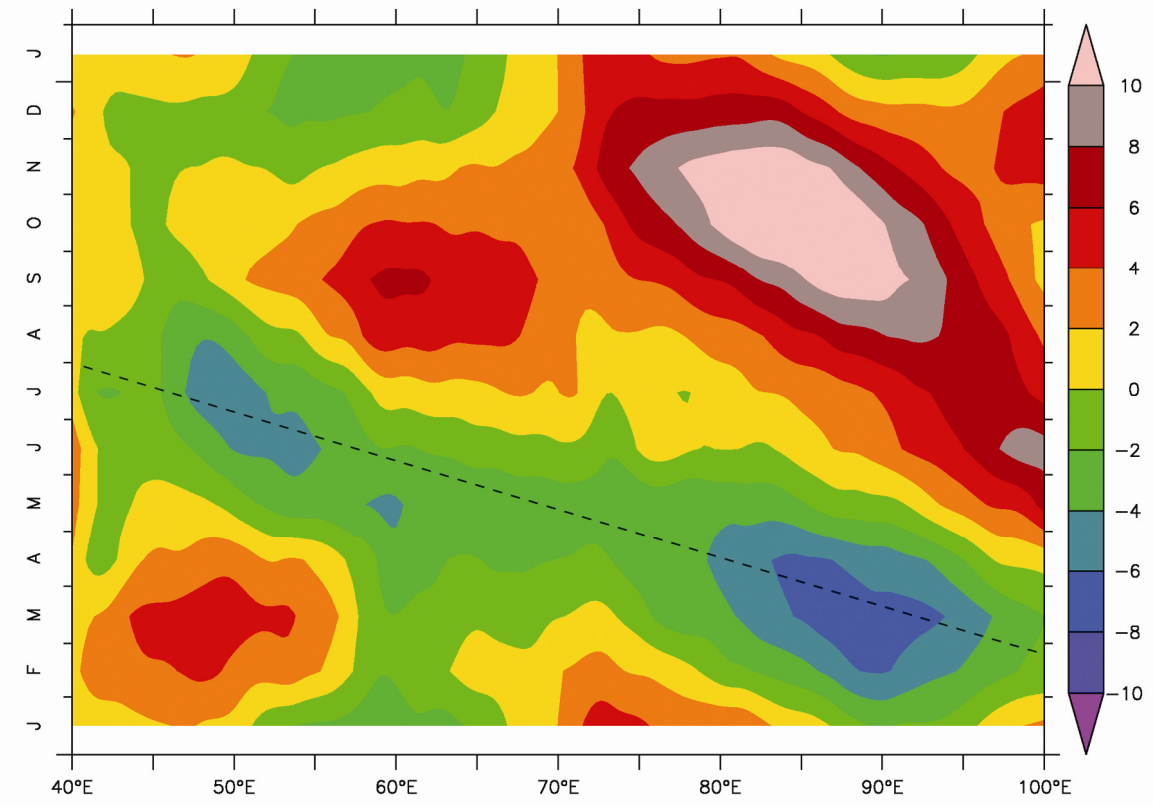

Figure 4. Hovmöller diagram of monthly climatological sea-level anomaly (cm) averaged over 5°–10°S. The dashed line represents the slope of wave pattern.

and shows a decreasing trend in WSCTR, the thermocline is still shallow (~54 m). One reason can be the natural lag that exists between the atmospheric forcing and oceanic response. However, thermocline variability is also associated with baroclinic Rossby waves whose propagation can delay the oceanic feedback to the atmospheric forcing[25]. During May–July, upwelling Rossby waves in ESCTR destructively interfere with the downward Ekman pumping and inhibit/reduce the downwelling[1,5]. Figure 4 shows the Hovmöller diagram of monthly climatological SLA averaged over 5°–10°S. The figure clearly suggests westward propagation of SLA. Phase speed of the propagation calculated from slope of the wave pattern is ~38 cm/s. The theoretical phase speed of first-mode baroclinic Rossby wave is given as $Cr = B * C^2/f^2$, where Cr is the phase speed of Rossby waves, C the long internal gravity wave speed, f the Coriolis parameter and β is the meridional gradient of f. The characteristic speeds (C) for the first baroclinic modes[26] have been calculated as 258 cm/s. The first baroclinic Rossby wave speed at 8°S is calculated to be 38 cm/s. Thus, it appears that the westward-propagating SLA signal on seasonal scale is the first mode baroclinic oceanic Rossby wave[27]. These upwelling (characterized by negative SLA) and downwelling (characterized by positive SLA) Rossby waves can move up and down the thermocline respectively. It may be noted that Rossby waves have interannual variability associated with Indian Ocean dipole, La-Niña, El-Niño, etc.[28–30].

Other than winds, stratification also plays a major role in determining the depth mixed layer[31]. Strong stratification can be a result of high buoyancy at the surface layer, which is eventually determined by sea-surface temperature (SST) and sea-surface salinity (SSS). Figure 5 shows the monthly climatological surface salinity distribution in the Indian ocean overlaid by the OSCAR ocean surface currents. During November–March, the SCTR is characterized by low-saline (<34.5) surface waters advected from the east. The low-saline waters from the Pacific are carried into the SCTR by the westward-flowing South Equatorial Current (SEC), typically observed south of 5°S. These low-saline waters are again freshened by rainfall in SCTR and west of SCTR[2,32]. Presence of low-saline waters from the Bay of Bengal has also been documented in SCTR[33]. During southwest monsoon (June–August), the core of SEC shifts further south (south of 10°S) and surface waters in SCTR are contributed mainly by the meridional flow of high-saline waters from the Arabian Sea[6]. Previous studies also suggest that SSS variability in SCTR is mainly regulated by the ocean surface currents[14,24,32].

Figure 6 *a* and *b* shows the depth–time plots of salinity averaged over WSCTR and ESCTR. It can be seen that

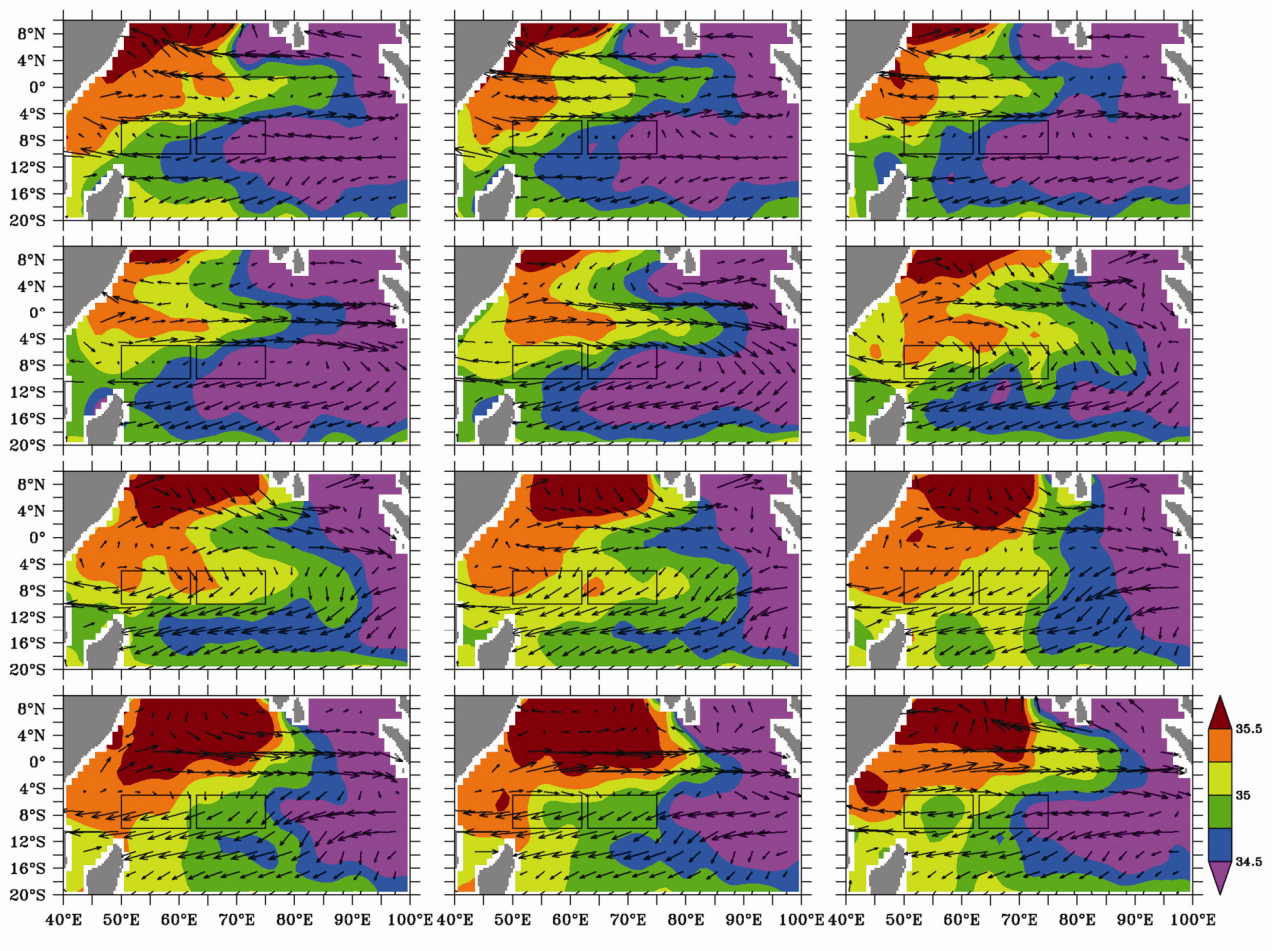

Figure 5. Monthly climatological surface salinity distribution in the Indian Ocean overlaid by the OSCAR ocean surface currents (m/s).

except during July–September, the SCTR is capped by low-saline (<35.2) tropical surface water[32] over the high-saline (>35.25) subsurface water. Further, WSCTR is ~0.3 units more saline than ESCTR. The main reason for this is the intrusion of fresher water from the east to ESCTR than to WSCTR. Additionally, in WSCTR meridional intrusion of high-saline water is more than that in ESCTR (Figure 5). The temperature depth–time plots averaged over WSCTR (Figure 6 *c*) and ESCTR (Figure 6 *d*) show more or less similar nature with high SST (~28°C) from November to May. However, from June to October, SST is lower (~26°C) in WSCTR compared to ESCTR (~27°C). Figure 6 *e* and *f* shows the monthly climatological Brunt–Vaisala frequency depth–time plot averaged over WSCTR and ESCTR respectively. It clearly shows a highly stratified ocean during November to May and weak stratification during June to September. It is also evident from the figure that ESCTR is more stratified than WSCTR, and that chl *a* concentration is more when the stratification is weak. The low stratification observed is clearly associated with the high-saline and low-temperature surface waters during June–September. At the surface layer of the ocean, heat gain (surface warming) or precipitation tends to make it more buoyant and contributes to the stratification. On the other hand, surface cooling or evaporation contributes to the loss of buoyancy and makes the surface layer denser than the subsurface layer causing convective overturning, which results in mixing. Winds can also cause overturning and mixing through the sheared flow instability. The stratification in SCTR is further aided by wind pattern (weak winds during November to May and strong winds during June to October; Figure 3 *e*). This wind- or buoyancy-generated mixing can entrain the subsurface properties (temperature, salinity, nutrients, chl *a*, etc.) to the surface and thus modify the surface layer. Weak stratification helps in entraining the nutrients to the surface, where light is not limited and chl *a* concentration is increased.

It is clear from seasonal variation of SST and SSS (Figure 7 *a* and *b*) that low SSS and high SST during November–May support strong stratification, while high SSS and low SST support weak stratification from June to October in SCTR. The rain rate averaged over WSCTR and ESCTR (Figure 7 *c*) also supports the

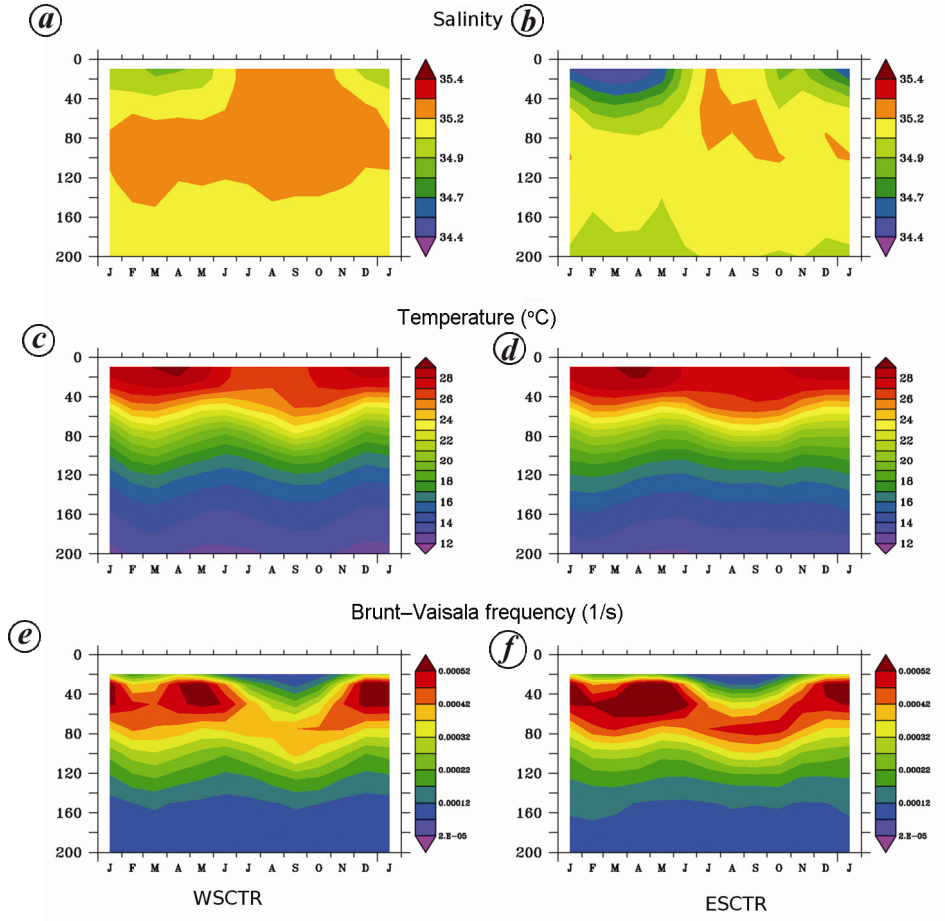

Figure 6. Depth–time plot of salinity averaged over: ***a***, WSCTR (50°–62°E, 5°–10°S); ***b***, ESCTR (63°–75°E, 5°–10°S). Depth–time plot of temperature (°C) averaged over; ***c***, WSCTR; ***d***, ESCTR. Depth–time plot of Brunt–Vaisala frequency (1/s) averaged over; ***e***, WSCTR (50°–62°E, 5°–10°S); ***f***, ESCTR (63°–75°E, 5°–10°S).

observed variation in SSS, with minimum rain rate in July–August. Stratification is the combined effect of wind and buoyancy forcing. It is of interest to quantify the contribution from wind and buoyancy forcing towards the observed stratification. Figure 7 *d* shows the climatological friction velocity averaged over WSCTR and ESCTR, which is proportional to the energy imparted from the atmosphere to the ocean[34]. It is clearly seen that during the high chl *a* period, friction velocity is at its maximum and in WSCTR it is more than that in ESCTR. Figure 7 *e* shows the surface buoyancy flux averaged over WSCTR and ESCTR. In WSCTR, the buoyancy flux has its minimum in June and in ESCTR, the minimum is in July. Clearly, the buoyancy flux and winds support weak stratification in the SCTR during the elevated chl *a* period. Figure 7 *f* shows the saline contribution to the buoyancy flux. It is evident from the figure that the saline contribution to buoyancy flux is less than that compared to the thermal contribution (Figure 7 *g*). The observed dip in buoyancy flux during June–September is associated with low or negative net heat flux in the region[35] (Figure 7 *h*). The surface PAR averaged over WSCTR and ESCTR ranges from ~36 to ~48 Einstein/m^2/day (Figure 7 *i*). Latelier *et al.*[36] used surface PAR value less than 32 (Einstein/m^2/day) to represent the less productive winter light condition in the North Pacific subtropical gyre. The satellite-derived surface PAR values noted in WSCTR and ESCTR were always greater than 32 Einstein/m^2/day and reached 48 Einstein/m^2/day. Further, maximum chl *a* concentration was noted during the boreal summer when the surface PAR was at its lowest. This indicates that seasonal variability of the surface PAR may not be the governing factor for the observed chl *a* variability. Thus it is clear that the weak stratification and increased wind forcing result in elevated summer chl *a* concentration in the SCTR.

The depth at which the wind-generated turbulence is balanced by the surface buoyancy can be represented by Monin–Obukhov length (L). The ratio of L and MLD can suggest if the mixed layer is dominated by wind mixing ($|L/MLD| > 1$) or weak wind mixing confined by buoyancy effects[37] ($|L/MLD| < 1$). Figure 8 shows the $|L/MLD|$ variability averaged over WSCTR and ESCTR. From the figure, it is clear that from April to September, the

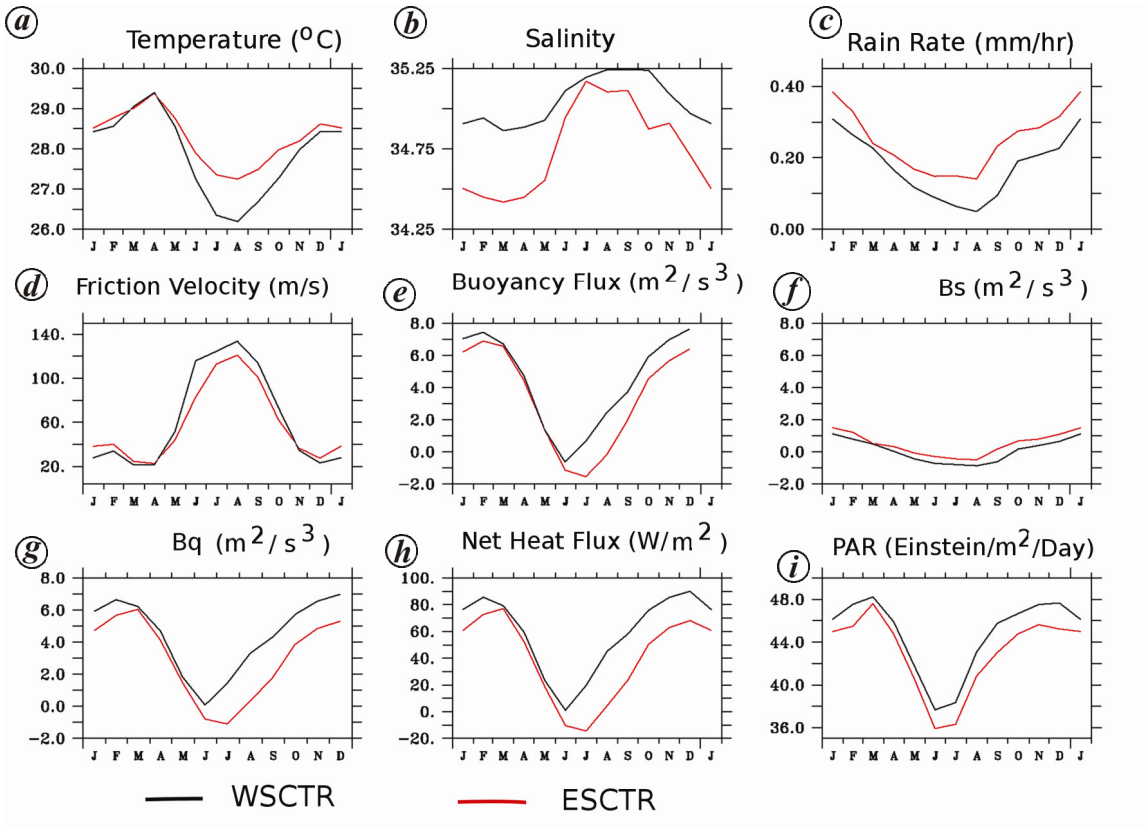

Figure 7. Annual variation of various parameters averaged over WSCTR (black line, 50°–62°E, 5°–10°S) and ESCTR (red line, 63°–75°E, 5°–10°S). ***a***, Temperature (°C); ***b***, salinity; ***c***, rain rate (mm/h); ***d***, friction velocity U^3* (m/s) × 10^{-8}; ***e***, Buoyancy flux (m^2/s^3); ***f***, Haline buoyancy flux (m^2/s^3); ***g***, thermal buoyancy (m^2/s^3); ***h***, net heat flux (W/m^2); ***i***, PAR (Einstien/m^2/day).

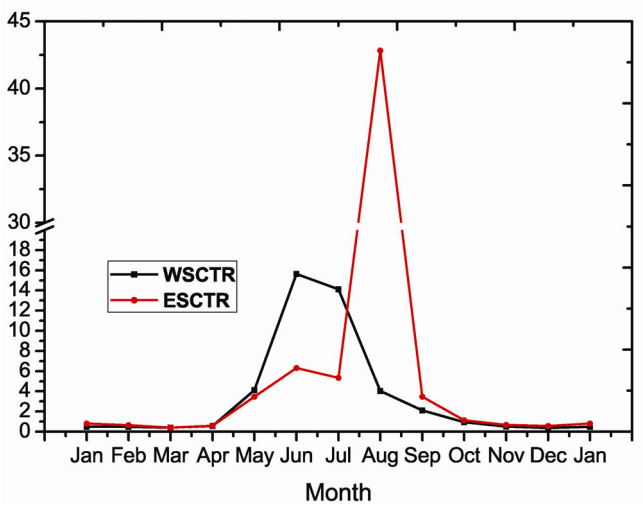

Figure 8. Annual variation of ratio of Monin–Obukhov length (*L*) and mixed layer depth (*MLD*).

|*L*/*MLD*| values are greater than 1 and mixed layer is dominated by wind mixing both in WSCTR and ESCTR. However, from November to March, the |*L*/*MLD*| values are less than 1 when the wind energy is less and net buoyancy flux values is high (Figure 7 *e*). This indicates that wind mixing is confined by strong surface stratification. Our analysis of the climatological dataset clearly suggested that wind mixing has a major role in the deepening of MLD, supported by convective mixing in the boreal summer. The sea-truth CTD, chl *a* and nitrate observations carried out during November 2008 and June 2009 at 8°S, 65°E demonstrate the relationship between physical variables and chl *a* (Figure 9). It can be seen that at thermocline depth, nitrate values are greater than 1 µM/l and when MLD reaches the nitrate-rich thermocline waters, surface chl *a* also increases. Figure 9 *a* shows the potential density and Brunt–Vaisala frequency profile derived from CTD measurements at 8°S, 65°E during November 2008 and June 2009. It is clear from the figure that the MLD/pycnocline is shallow (10/25 m) during November and deep (40/50 m) during June, similar to that observed in the climatological dataset. The chl *a* and nitrate data (Figure 9 *b*) collected along with the CTD profiles suggest that during November, surface chl *a* is less (~0.15 mg/m^3) and during June it is more (~0.3 mg//m^3). As mentioned earlier, the elevated surface chl *a* during June can be a result of deep MLD reaching the nitrate-rich thermocline region and increased entrainment of nutrients to the surface. On the other hand, during November, MLD does not reach the nutrient-rich thermocline region and surface layers are nutrient-limited[24]. The weak/strong Brunt–Vaisala frequency during

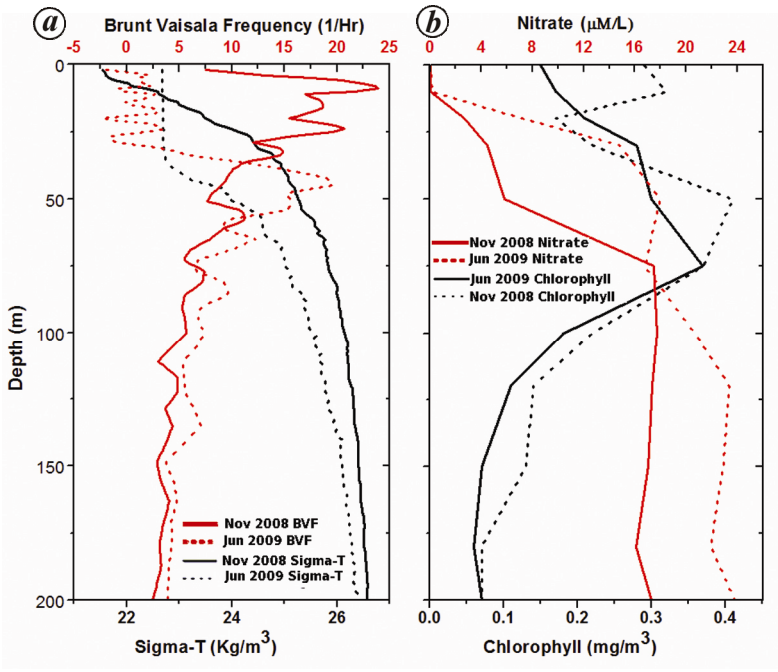

Figure 9. ***a***, The potential density (kg/m^3) and Brunt–Vaisala frequency (1/h) profile derived from CTD measurement at 8°S, 65°E during November 2008 and June 2009. ***b***, Chlorophyll *a* (mg/m^3) and nitrate (μM/L) concentration profile collected at 8°S, 65°E during November 2008 and June 2009.

June/November indicates weak/strong stratification in the water column. The presence of low-/high-saline surface water and weak/strong wind stress from QuikSCAT (0.04/0.1 N/m^2, figure not shown) supports the observed shallow/deep MLD during November/June. The *in situ* observations also justify that the thermocline defined by 23°C isotherm depth is nutrient rich (>1 μM/l).

In order to further show the role of different physical processes on the seasonal cycle of chl *a* concentration, monthly climatology of physical variables averaged over WSCTR/ESCTR was correlated with monthly climatological SeaWiFS surface chl *a* (Figure 10). In the figure, each dot represents the monthly climatology of the respective oceanographic variables averaged over ESCTR (red dots) and WSCTR (black dots). Figure 10 *a* shows the regression of climatological SeaWiFS surface chl *a* and thermocline depth averaged over WSCTR/ESCTR. The figure suggests a direct relationship, but the correlation coefficient is weak ($R = 0.31/0.41$) and not significant ($P \le 0.3/0.2$). However, correlation between surface chl *a* and MLD in WSCTR/ESCTR shows a direct relationship (Figure 10 *b*) with strong correlation coefficient ($R = 0.9/0.86$) and significance ($P \le 0.01/0.01$). The observed strong inverse correlation between surface chl *a* and SST ($R = -0.93/-0.89$, $P \le 0.01/0.01$) in WSCTR/ESCTR and positive correlation between surface chl *a* and SSS ($R = 0.81/0.84$, $P \le 0.01/0.01$) indicate the possible role of SST and SSS on observed MLD (Figure 10 *c* and *d* respectively). Correlation between rain rate and surface chl *a* also shows an inverse relationship ($R = -0.80/0.66$, $P \le 0.01/0.02$) in WSCTR/ESCTR region (Figure 10 *e*). An inverse relationship ($R = -0.80/-0.66$, $P \le 0.02/0.01$) is also observed between buoyancy flux and surface chl *a* in WSCTR/ESCTR (Figure 10 *f*). SST, SSS and rain rate eventually influence buoyancy flux and hence MLD. Strong direct correlation ($R = 0.96/0.97$, $P \le 0.01/0.01$) between friction velocity and surface chl *a* suggests wind mixing as a major contributior to the observed chl *a* variability (Figure 10 *g*). An inverse correlation is observed between surface PAR and surface chl *a* ($R = -0.59/-0.84$, $P \le 0.04/0.01$) in WSCTR/ESCTR, suggesting that PAR may not be an important parameter for the observed chl *a* (Figure 10 *h*). Correlation between surface chl *a* and Ekman pumping also shows an inverse relationship ($R = -0.49/-0.89$, $P \le 0.1/0.01$), suggesting that wind-induced upwelling maintains a shallow thermocline in WSCTR/ESCTR, but has a small role in the observed chl *a* variability (Figure 10 *i*).

Physical parameters and their relation to chl *a* in WSCTR and ESCTR show a similar picture in both the regions. The observed high amplitude of chl *a* variability in WSCTR during June–September could not be explained by the MLD variability alone. Waters around Chagos archipelago (~5°S, ~72°E) and Mascarene plateau (4°–20°S, ~56°E) are always characterized by elevated chl *a* in SCTR[10,32,38]. Some areas of elevated chl *a* in SCTR are related to ridges and islands (stars in Figure 2, GEBCO Atlas 2003). WSCTR is characterized by the presence of Mascarene plateau and many small islands[37]. These islands and ridges present in the plateau can help in breaking the internal waves and eventually

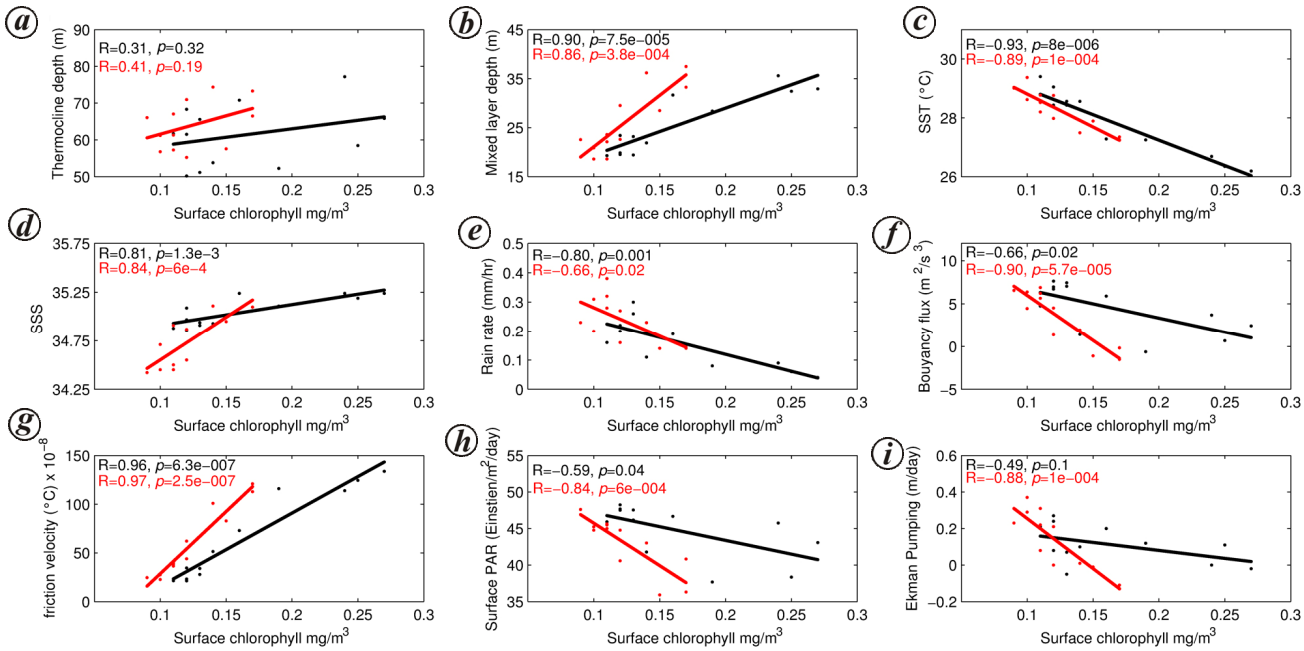

Figure 10. The scatter plot of monthly climatological physical parameters versus monthly climtological surface SeaWiFS chl averaged over WSCTR (black) and ESCTR (red). ***a***, Thermocline; ***b***, mixed layer depth; ***c***, SST; ***d***, SSS; ***e***, rain rate; ***f***, buyancy flux; ***g***, friction velocity; ***h***, PAR; ***i***, Ekman pumping. The thick lines represent the best fit.

cause turbulent diffusion of nutrients from the thermocline to the upper layers[39–41]. During the less stratified period when the winds are strong, this turbulent diffusion may be more, and results in high concentration of surface chl *a* as observed from June to September in WSCTR. Another mechanism of increased productivity in WSCTR is eddy shedding. When the currents become strong over the Mascarene plateau, eddies are generated supplying nutrients to the surface layers[38].

Conclusion

Seasonal variation of surface chl *a* concentration in the SCTR shows a weak semiannual signature. In spite of the year-round shallow thermocline prevalent in SCTR, elevated surface chl *a* concentration is noted only from June to October. This can be associated with the low stratification and deep mixed layer observed during this period. The deepening of MLD and low stratification influence the surface chl *a* variability in SCTR. This is mainly due to the shallow thermocline/nitracline prevailing in the region as a combined effect of Ekman pumping and upwelling Rossby waves. The low stratification and mixing can bring nutrients from the thermocline to the surface layers, and eventually chl *a* concentration will increase. Even though previous studies suggest that on a seasonal scale, MLD deepening is the key to chl *a* blooms in SCTR, what drives MLD deepening is not clear. Our analysis suggests that the observed low stratification and deep mixed layer are primarily due to wind mixing during March–October, whereas strong stratification observed in rest of the year is due to weak winds and strong surface buoyancy. The latter is attributed to surface warming due to net heat flux and presence of low-saline surface waters advected from the Pacific Ocean and Bay of Bengal along with the high rain rate in the SCTR. The stratification is weakened in SCTR by the net negative heat flux and meridional flow of high-saline water from the Arabian Sea into the SCTR. Another notable observation is that WSCTR has higher chl *a* concentration than ESCTR, and this could be due to the presence of the Mascarene plateau and many small islands. Further, WSCTR is less stratified than ESCTR, and the gap between the base of MLD and thermocline is less in WSCTR. It appears that the seasonal surface PAR variability may not play a significant role in seasonal variability of surface chl *a* in SCTR. It should be noted that SCTR is characterized by strong interannual variability in SST, MLD and Rossby waves[25] which in-turn may affect chl *a* distribution in the region. This needs to be addressed in future studies.

1. Hermes, J. C. and Reason, C. J. C., Annual cycle of the South Indian Ocean (Seychelles–Chagos) thermocline ridge in a regional ocean model. *J. Geophys. Res.*, 2008, **113**, C04035; doi:10.1029/2007JC004363.
2. Vialard, J. *et al.*, Air–sea interactions in the Seychelles–Chagos thermocline ridge region. *Bull. Am. Meteorol. Soc.*, 2009, **90**, 45–61.
3. Mccreary, J. P., Kundu, P. K. and Molinari, R. L., A numerical investigation of dynamics, thermodynamics and mixed-layer processes in the Indian Ocean. *Prog. Oceanogr.*, 1993, **31**, 181–244.
4. Yokoi, T., Tozuka, T. and Yamagata, T., Seasonal variation of the Seychelles dome. *J. Climate*, 2008, **21**, 3740–3754.
5. Kawamiya, M. and Oschlies, A., Formation of a basin-scale surface chl pattern by Rossby waves. *Geophys. Res. Lett.*, 2001, **28**, 4139–4142.

6. Schott, F. A., Xie, S. P. and Mccreary, J. P., Indian Ocean circulation and climate variability. *Rev. Geophys*., 2009, **47**, RG1002.
7. Mccreary, J. P. *et al.*, Biophysical processes in the Indian Ocean. In *Indian Ocean Biogeochemical Processes and Ecological Variability*, Geophysical Monograph Series 185, American Geophysical Union, Washington, DC, 2009, pp. 9–32.
8. Resplandy, L., Vialard, J., Lévy, M., Aumont, O. and Dandonneau, Y., Seasonal and intraseasonal biogeochemical variability in the thermocline ridge of the southern tropical Indian Ocean. *J. Geophys. Res*., 2009. **114**, C07024.
9. Beckmann, A. and Hense, I., Beneath the surface: characteristics of oceanic ecosystems under weak mixing conditions – a theoretical investigation. *Prog. Oceanogr*., 2007, **75**, 771–796.
10. Wilson, C. and Qiu, X., Global distribution of summer chl blooms in the oligotrophic gyres. *Prog. Oceanogr.*, 2008, **78**, 107–134.
11. Vinayachandran, P. N. and Saji, N. H., Mechanisms of South Indian Ocean intraseasonal cooling. *Geophys. Res. Lett.*, 2008, **35**, L23607.
12. Waliser, D. E., Murtugudde, R., Strutton, P. and Li, J. L., Subseasonal organization of ocean chl: prospects for prediction based on Madden–Julian Oscillation. *Geophys. Res. Lett.*, 2005, **32**, L23602.
13. Jayakumar, A. and Gnanaseelan, C., Study the mechanism of surface chl *a* variability in the southern tropical Indian Ocean using an OGCM. *Mar. Geodesy*, 2012, **35**, 246–256; doi:10.1080/01490419.2011.637874.
14. Daria, H. and Tong, L., Mechanisms controlling seasonal mixed layer temperature and salinity in the southwestern tropical Indian Ocean. *Dyn. Atmos. Oceans*, 2011, **51**, 77–93.
15. Conkright, M. E., Locarnini, R. A., Garcia, H. E., O'Brien, T. D., Boyer, T. P., Stephens, C. and Antonov, J. I., *World Ocean Atlas 2001: Objective Analyses, Data Statistics, and Figures*, CD-ROM Documentation, National Oceanographic Data Center, Silver Spring, MD, 2002, p. 17.
16. Shigeki, H., Ohira, T. and Nakamura, T., A monthly mean data set of global oceanic temperature and salinity derived from Argo float observations. JAMSTEC Report of Research Development, 2008, vol. 8, pp. 47–59.
17. Simons, R. A., ERDDAP – The Environmental Research Division's Data Access Program, NOAA/NMFS/SWFSC/ERD, Pacific Grove, CA, USA; http://coastwatch.pfeg.noaa.gov/erddap
18. Bonjean, F., and Lagerloef, G. S. E., Diagnostic model and analysis of the surface currents in the tropical Pacific Ocean. *J. Phys. Oceanogr*., 2002, **32**, 2938–2954.
19. Yu, L., Jin, X. and Weller, R. A., Global Flux Datasets from the Objectively Analyzed Air-sea Fluxes (OAFlux) Project: latent and sensible heat fluxes, ocean evaporation, and related surface meteorological variables. OAFlux Project Technical Report OA-2008-01, Woods Hole Oceanographic Institution, Woods Hole, Massachusetts, USA, 2008, p. 64.
20. Strickland, J. D. H. and Parsons, T. R., A practical handbook of seawater analysis. *Can. Bull. Fish. Aquat. Sci.*, 1972, **167**, 310.
21. Weller, R. A., Baumgartner, M. F., Josey, S. A., Fischer, A. S. and KIndle, J. C., A one-year record of atmospheric forcing from the Arabian Sea. *Deep Sea Res*., 1998, **45**, 1961–1999.
22. Pond, S. and Pickard, G. L., *Introductory Dynamic Oceanography*. Pergamon Press, New York, 1978.
23. Gill, A. E., *Atmosphere–Ocean Dynamics*, Acadamic Press, New York, USA, 1982, p. 662.
24. George, J. V. *et al.*, Role of physical processes in chlorophyll distribution in the western tropical Indian Ocean. *J. Mar. Syst*., 2013, **113**, 1–12.
25. Xie, S. P., Annamali, H., Schot, F. A. and McCreary Jr, J. P., Structure and mechanisms of South Indian Ocean climate variability. *J. Climate*, 2002, **15**(8), 864–878.
26. McCreary, J. P., Equatorial beams. *J. Mar. Res*., 1984, **42**, 395–430.
27. Matano, R. P., Beier, E. J., Strub, P. T. and Tokmakian, R., Large-scale forcing of the Agulhas variability: the seasonal cycle. *J. Phys. Oceanogr*., 2002, **32**, 1228–1241.
28. Saji, N. H., Xie, S.-P. and Tam, C.-Y., Satellite observations of intense intraseasonal cooling events in the tropical south Indian Ocean. *Geophys. Res. Lett*., 2006, **33**, L14704; doi:10.1029/2006GL026525.
29. Murtugudde, R., Mccreary, J. P. and Busalacchi, A. J., Oceanic processes associated with anomalous events in the Indian Ocean with relevance to 1997–1998. *J. Geophys. Res.*, 2000, **105**, 3295–3306.
30. Wiggert, J. D., Murtugudde, R. G. and Mcclain, C. R., Processes controlling interannual variations in wintertime (northeast monsoon) primary productivity in the central Arabian Sea. *Deep Sea Res*., *Part II*, 2002, **49**, 2319–2343.
31. Keerthi, M. G., Lengaigne, M., Vialard, J., De Boyer Montégut, C. and Muraleedharan. P. M., Interannual variability of the tropical Indian Ocean mixed layer depth. *Climate Dyn*., 2013, **40**, 743–759.
32. New, A., Alderson, S., Smeed, D. and Stansfield, K., On the circulation of water masses across the Mascarene Plateau in the South Indian Ocean. *Deep Sea Res*., 2007, **54**, 42–74.
33. Sengupta, D. G. N., Bharath Raj and Shenoi, S. S. C., Surface freshwater from Bay of Bengal runoff and Indonesian throughflow in the tropical Indian Ocean. *Geophys. Res. Lett*., 2006, **33**, L22609.
34. Foltz, G. R., Vialard, J., Praveen Kumar, B. and McPhaden, M. J., Seasonal mixed layer heat balance of the southwestern tropical Indian Ocean. *J. Climate*, 2010, **23**, 947–965; doi:10.1175/2009JCLI3268.1.
35. Yokoi, T., Tozuka, T. and Yamagata, T., Seasonal and interannual variations of the SST above the Seychelles Dome. *J. Climate*, 2012, **25**, 800–814.
36. Latelier, R. M., Karl, D. M., Abott, M. R. and Bidigare, R. R., Light driven seasonal patterns of chlorophyll and nitrate in the lower euphotic zone of the North Pacific Subtropical Gyre. *Limnol. Oceanogr.*, 2004, **49**(2), 508–519.
37. Anitha, G., Ravichandran, M. and Sayanna, R., Surface buoyancy flux in Bay of Bengal and Arabian Sea. *Ann. Geophys*., 2008, **26**, 395–400; doi:10.5194/angeo-26-395-2008.
38. New, A. L., Stansfield, K., Smythe-wright, D., Smeed, D. A., Evans, A. J. and Alderson, S. G., Physical and biochemical aspects of the flow across the Mascarene Plateau in the Indian Ocean. *Philos. Trans. R. Soc. London, Ser. A*, 2005, **363**, 151–168.
39. Konyaev, K. V., Sabinin, K. D. and Serebryany. A. N., Large-amplitude internal waves at the Mascarene Ridge in the Indian Ocean. *Deep Sea Res. Part I,* 1995, **42**, 2075–2091.
40. Morozov, E. G. and Vlasenko, V. I., Extreme tidal internal waves near the Mascarene Ridge. *J. Mar. Syst*., 1996, **9**, 203–210.
41. Wunsch, C. and Ferrari. R., Vertical mixing, energy, and the general circulation of the oceans. *Annu. Rev. Fluid Mech*., 2004, **36**, 281–314.

ACKNOWLEDGEMENTS. This study was supported by the Ministry of Earth Sciences, Government of India. We thank the Director, NIOT, Chennai and Director, NCAOR, Goa for support and Dr C. T. Achuthankutty (Visiting Scientists, NCAOR, Goa) for suggestions to improve the manuscript. The Argo data were collected and made available freely by the International Argo Program and the national programmes that contribute to it. This is NCAOR contribution no 29/2017.

Received 24 June 2015; revised accepted 14 September 2017

doi: 10.18520/cs/v114/i04/868-878